NUMERICAL MODELING OF SEVERAL CASEC OF THE STRATIFIED FLOW

L. Beneš [1]

Summary: *The article deals with the numerical simulation of the stratified incompressible flows over the body and over the isolated hill. The mathematical model is based on the Boussinesq approximation of the Navier–Stokes equations for viscous incompressible flow wit non–constant density. Three different numerical approaches to the body are implemented and tested. The first one is the classical body fitted mesh. The second one is based on the penalization technique and the obstacle is modeled as the permeable body with high resistance parameter. The last approach is based on the immersed boundary method. Different boundary conditions on the outlet are tested. The resulting set of PDE's is then solved by the AUSM MUSCL scheme in finite volume approximation. For the time integration the three stage BDF method of the second order is used.*

Key words: stratification, obstacle modeling, AUSM MUSCL

1. Introduction

Modeling of the stratified flows plays a significant role in many engineering and environmental applications (e.g. stratification affects the transport of pollutants, plays significant role in determining the consequences of accidents on environment and human etc.). Study of stratified flows has a long tradition. The beginning of the studies of internal waves, produced by a flow over topography or body, moving in stratified liquid, is dating back to XIX century and is still continuing.

Often, the flow can be assumed to be incompressible. Nevertheless, the density is not constant owing to temperature changes, salinity, gravity, etc. The main phenomena, which are not presented in the constant density case, are internal waves and anisotropic mixing, jet–like flow structures, thin interfaces with high density and velocity gradients and anisotropic turbulence. All phenomena are important in environment and technology. The well–known case of internal waves are Lee waves, which are generated whenever the fluid is flowing past isolated obstacles.

The experimental and numerical studies of the flow around a moving obstacle were proposed by e.g. (1),(4),(21), (6),(5),(16),(7).

From the numerical point of view, the simulations of stratified fluid flows are in general more demanding than the solution of similar non-stratified flow cases. The transport equation for the

[1] Doc. Ing. Luděk Beneš PhD Dept. Of Technical Mathematics, Faculty of Mechanical Engineering, Czech Technical University in Prague, Karlovo nám 13, 121 35, Prague 2, tel. +420 224357543, e-mail benes@marian.fsik.cvut.cz

density (or its perturbation) is coupled to momentum equations by a buoyancy term. Because of this buoyant force the obstacles in flow generate waves that propagate at long distances. These waves need to be properly resolved, without unphysical damping or dispersion.

Our study of the stratified flow started in 2008 by the simulation of the flow past a ball in 2D (14) using WENO, AUSM MUSCL and compact differences schemes . The extension to 3D was published in (12), (13). Next studies were devoted to the flow around thin vertical strip (15) and over sinusoidal hill (9).

The correct resolution of the flow structure over the body can be affected by its representation. Suitability of different body's models can also depend on the effects under investigation. It means whether we are interested more in the boundary layer in the proximity of the body surface or rather in the development of internal waves farther from the body. Different methods of body's modeling are presented in this paper.

The second significant question are appropriate boundary conditions. Three different boundary conditions are implemented and compared in the case of the flow over isolated hill.

2. Mathematical model

We have supposed flow in the ABL as viscous and incompressible. But the density is not constant due to gravity force. As the mathematical model the system of Navier-Stokes equations for viscous incompressible flow with variable density was used. These equations are simplified by the Boussinesq approximation. Density and pressure are divided into two parts: a background field (with subscript $_0$) plus a perturbation. The momentum equations are partly linearized around the average state ρ_*. The resulting set of equations can be written in the form

$$\frac{\partial \varrho}{\partial t} + \frac{\partial(\varrho u_j)}{\partial x_j} = -u_2 \frac{\partial \varrho_0}{\partial x_2}, \tag{1}$$

$$\frac{\partial u_i}{\partial t} + \frac{\partial(u_j u_i)}{\partial x_j} + \frac{1}{\varrho_*}\frac{\partial p}{\partial x_i} = K\frac{\partial^2 u_i}{\partial x_j\, \partial x_j} - \delta_{i,2} g, \tag{2}$$

$$\frac{\partial u_j}{\partial x_j} = 0, \tag{3}$$

where $W = [\varrho, u_1, u_2, p]^T$ is the vector of unknowns, $\varrho(x_1, x_2, t)$ denotes the perturbation of the density and u_1, u_2 are the velocity components, p stands for the pressure perturbation and g for the gravity acceleration. The x_1–axis is orientated in the direction of the motion and the x_2–axis is perpendicular to the density gradient.

For the description of the stratified flows with characteristic velocity U and characteristic length L following similarity numbers have been used:

$$Re = \frac{UL}{\nu}, \qquad\qquad Ri = -\frac{g}{\varrho_*}\frac{\frac{\partial \varrho_0}{\partial z}}{U}. \tag{4}$$

3. Numerical scheme

The AUSM MUSCL scheme in the finite volume formulation has been used for solution of the mentioned problems. For validation of obtained results the other two different schemes have

been used in the selected cases. The first of this schemes is the WENO scheme combined with the projection method, the second scheme is the compact finite–difference scheme. All schemes were validated in our previous studies. The schemes have been successfully used for simulation of the flow field around moving bodies in 2D and 3D stratified fluid for wide range of Richardson numbers see (12), (13), (14), (15).

• **AUSM scheme**

The second scheme is based on the artificial compressibility method in dual time. The continuity equation (3) is rewritten in the form

$$\frac{\partial p}{\partial \tau} + \beta^2 \frac{\partial u_j}{\partial x_j} = 0, \tag{5}$$

where τ is the artificial time.

The finite volume AUSM scheme is used for the spatial semidiscretization of the inviscid fluxes. Quantities $(q)_{L/R}$ on the left/right hand side of the face are computed using the MUSCL reconstruction with the Hemker-Koren limiter(20)

$$q_R = q_{i+1} - \frac{1}{2}\delta_R \quad q_L = q_i + \frac{1}{2}\delta_L,$$

$$\delta_{L/R} = \frac{a_{L/R}(b_{L/R}^2 + 2) + b_{L/R}(2a_{L/R}^2 + 1)}{2a_{L/R}^2 + 2b_{L/R}^2 - a_{L/R}b_{L/R} + 3},$$

$$a_R = q_{i+2} - q_{i+1} \quad a_L = q_{i+1} - q_i \quad b_R = q_{i+1} - q_i \quad b_L = q_i - q_{i-1}.$$

The scheme is stabilized according to (10) by the pressure diffusion.

$$\begin{pmatrix} 0 \\ 0 \\ 0 \\ \eta \frac{p_{i+1,j} - p_{i,j}}{\beta_x} \end{pmatrix} \qquad \beta_x = w_r + \frac{2\nu}{\Delta x}$$

where w_r is reference velocity (in our case the maximum velocity in flow field).

The viscous fluxes are discretized using central approach on a dual mesh (diamond type scheme).

The spatial discretization results in a system of ODE's solved by the second-order BDF formula

$$\frac{3W^{n+1} - 4W^n + W^{n-1}}{2\Delta t} + L^{n+1} = 0. \tag{6}$$

Here, L^{n+1} denotes the numerical approximation of the convective and viscous fluxes described above and the source terms. Arising set of nonlinear equations is then solved by the artificial compressibility method in the dual time τ by the explicit 3-stage second-order Runge-Kutta method.

4. Computational setup

The presented computational setup corresponds to the experimental setup studied by Chaschechkin and Mitkin in (16).The gravity waves are generated by the moving of the thin horizontal strip

$0.025 \times 0.002\ m$ in the towing tank. The dimensions of the tank are $2.2 \times 0.6\ m$. The strip is located $1m$ from the left wall and at the mid–heights. At the time $t = 0$ the obstacle starts moving to the right (in the positive x_1 direction) with constant velocity $U^{ob} = 0.0017\ m/s$. The flow field is initially at rest with the exponential profile of stratification $\varrho_0 = \varrho_{00} \exp \frac{x_2}{\Lambda}$, $\varrho_{00} = 1008.9\ kg/m^3$, $\Lambda = 47.735\ m$, the kinematic viscosity is $\nu = 10^{-6} m^2/s$. In our computations the body is fixed in the incoming flow of the corresponding velocity and stratification given by the experiment.

The computational domain is $0.5 \times 0.25m$. The obstacle is placed $0.3m$ from the left side (ranges in $< 0.3; 0.325 > m$) and in the middle height. The origin is placed on the left side of the domain and in the middle height. The x_1 axis is orientated in the stream-wise direction.

The same set of the boundary conditions is satisfied in the physical and artificial time. On the inlet, the velocity is prescribed. Pressure and density disturbances are extrapolated from the flow field. On the outlet velocity and density perturbance are extrapolated. Pressure perturbance is set to zero. On the top and bottom, homogeneous Neumann boundary conditions are satisfied. Pressure is fixed in one point. In the multidomain case, the non–slip boundary conditions are prescribed for velocity component on the body. For the pressure and density perturbations the homogeneous Neumann condition are used.

The computations have been performed on the Cartesian mesh of 500×500 cells. The resolution of the mesh is $1mm$ in the x_1 direction and $0.5mm$ in the x_2 direction. To verify independence of the solution on the mesh, the mesh two times refined in each direction was used.

Three different numerical approaches of the body is studied an compared each to other.
• In the first case the classical body fitted mesh surrounding the obstacle is used. Very simple Cartesian grids consisting of four parts can be used due to the simplicity of the problem. In the case of the general body, the deformation of the mesh will play significant role in the numerical simulations.
• In the second case, the obstacle is modeled as a source term emulating a porous media with small permeability by the volume penalization technique. The momentum equations are modified by adding of the term proportional to the difference between the fluid and obstacle velocities.

$$\frac{\chi(x, y, t)}{K_{rez}}(U_i^{ob} - u_i), \tag{7}$$

where K_{rez} corresponds to the small permeability of the obstacle, moving with velocity U^{ob}, $\chi(x, y, t)$ is the characteristic function of the obstacle and is equal to 1 inside the obstacle and 0 elsewhere. The sensitivity of the model on the permeability parameter was studied in (12).
• The third model is simple variant of the immersed boundary method (18), (17). The velocities in the cells lying in the obstacle are set to zero, while pressure and density are computed for whole domain. This technique was successfully used in our previous computations (23).

The second computational case is given by the low smooth sine-shaped hill. The domain has dimensions $90 \times 30\, m$. The hill height is $h = 1m$.

The background density field is given by $\varrho_0(x_2) = \varrho_w + \gamma x_2$ with $\varrho_w = 1.2\, kg \cdot m^{-3}$ and $\gamma = -0.01\, kg \cdot m^{-4}$, the viscosity $\nu = 0.001$. Similar case was solved for wide range of Richardson numbers in (8). In the presented study, the influence of the outlet boundary conditions on the generation of the gravity waves was tested. For the numerical simulations the case with $g = -50 ms^{-2}$ which corresponds to the Richardson number $Ri = 0.5$ was used.

The computations have been performed on structured non–orthogonal grid. The grid consist of 233×117 points refined near the ground and in the vicinity of the hill. The minimal resolution in the x_2 direction is $\Delta x_2 = 0.03m$.

The following boundary conditions are satisfied. On the inlet the velocity profile is given by the relation $u_1(x_2) = U_0(x_2/H)^{1/r}$ where $U_0 = 1m/s$ and $r = 40$ was prescribed, $u_2 = 0$, $\rho = 0$ and pressure perturbation is extrapolated. Homogeneous Neumann conditions are satisfied on the top. No–slip boundary conditions for the velocity components are prescribed and homogeneous boundary conditions for pressure and density perturbations are prescribed on the ground. The three different boundary conditions are prescribed on the outlet.
•**BC1:** homogeneous Neumann condition are prescribed for velocity components and pressure perturbations. Pressure is set zero (homogeneous Dirichlet b.c.).
•**BC2:** advection equation $\frac{\partial q}{\partial t} + U_a \frac{\partial q}{\partial x} = 0$ is satisfied for $q = u_1, u_2, \varrho$, pressure is set zero. The advection velocity U_a is computed as the mean value of the u_1 velocity component on the inlet.
•**BC3:** are similar to previous case, only pressure is extrapolated.

The computations have been performed on structured non–orthogonal grid. The grid consists of 233×117 points refined near the ground and in the vicinity of the hill. The minimal resolution in the x_2 direction is $\Delta x_2 = 0.03m$.

5. Numerical results

Fig.1 shows the process of the wave evolution in the form of isolines of u_2 velocity component for three different times. The multidomain approach is used. The flow pattern is typical for transient internal waves past an impulsively started body in stably stratified flow. Behind the obstacle the system of gravity waves is formed. The upstream disturbances are pronounced, which is typical for the flow with relatively low Froude number. Behind the obstacle strip with step–like density profile is formed.

Next two figures, Figs.2-3, display the comparison of the different obstacle approaches in the form of the isolines of the relative error. The multidomain approach is chosen as the basic setup for comparison. Differences are normalized by the maximum quantity in the multidomain case. First of these shows u_2–velocity component, the second one distribution of the density perturbance. The higher differences are in the porous media approach. The main differences are in the vicinity of the corners. In the immersed boundary case the error is approximately the same on the leading and trailing edge. In the porous media case the relative error is significantly greater on the leading edge and in the wake behind the obstacle. The differences on the sides of the obstacle are relatively small.

Figs.4–5 displays the perpendicular distribution of the computed quantities in different distances. Point $x = 0.24m$ is in front of the obstacle, $x = 0.305m$ and $x = 0.315m$ are on the obstacle and $x = 0.35m$ is behind the obstacle. As is shown, the computed wave length is the same in all models and is in a good agreement with the Brunt-Väisälä frequency. Maxima and minima of all computed quantities are the highest in the multidomain approach mainly in front of and behind the obstacle. Results in the porous and immersed boundary cases are very similar. The boundary layer on the sides of the obstacle is well resolved in all approaches, see Fig.5b. Higher differences are in the density perturbance ϱ and in the u_2–velocity component.

Next comparison is given in the Tab.1. The maxima of the quantities in whole computational domain are summarized. These maxima are compared to the multidomain approach. Their

values are approximately 8% lower in the immersed boundary and porous case.

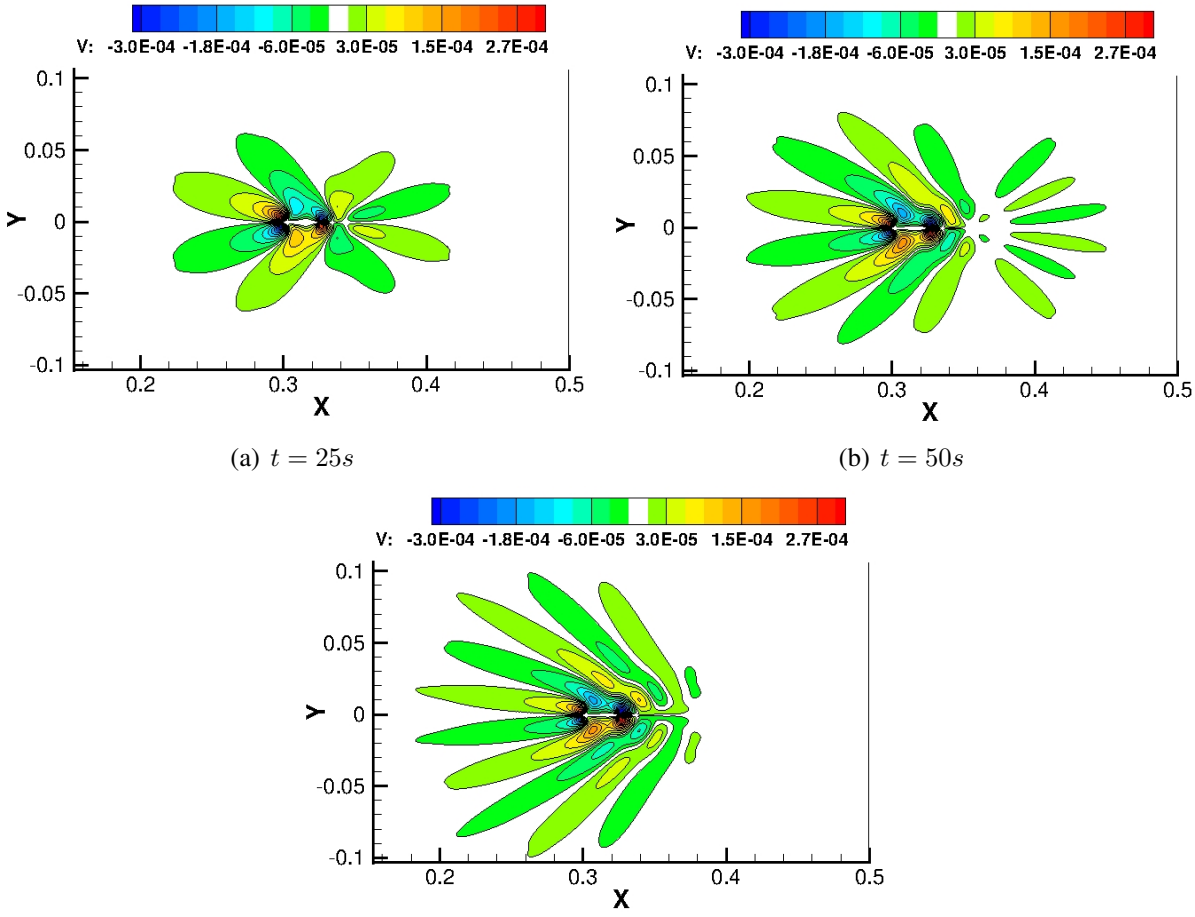

(a) $t = 25s$

(b) $t = 50s$

(c) $t = 75s$

Figure 1: Developing of the internal waves. Isolines of u_2– velocity component, three different times.

Fig. 6 displays the dependence of the flow on the boundary conditions. A comparison of the isolines of the u_2–velocity component for BC1 – BC3 is presented at the same time. The gravity waves with the wavelength given by the Brunt–Väisälä frequencies are visible. The results are affected by the boundary conditions on the inlet. The interaction of the wall with the inlet flow profile generates the wave pattern located close to the lower left corner. It is a local effect in the non–stratified case. In stratified one this perturbation generates the second system of gravity waves. This effect is strongest in the case BC3. The values of u_2 ranges for BC1,2 in $u_2 \in < -.228, 0.206 >$, for BC3 in $u_2 \in < -.154, 0.207 >$. Similarly also density perturbations are lover in BC3 case ($\varrho \in < -0.0065, 0.0165 >$ BC1,2, $\varrho \in < -0.0044, 0.0120 >$ BC3).

The BC1 and BC2 produce practically the same results. It is clearly visible in the Fig.7 where the relative error of the density perturbance ϱ and u_2–velocity component is shown. The differences are very small and are concentrated close to the ground behind the hill. On the other hand, BC3 generates different results. The waves on the inlet are significantly stronger in this case. Relative error to the BC1 case is shown in Fig.8. The differences are mainly close to the ground and in front of the hill. Also position of the waves are shifted.

It is also good visible in Figs.9,10, where the dependence of u_1 and ϱ in two different posi-

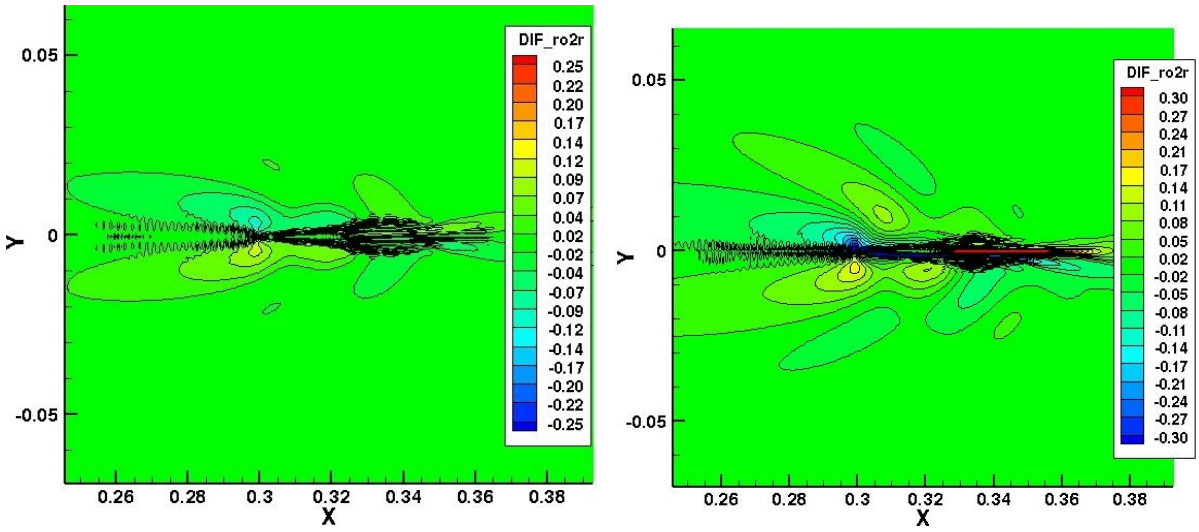

Figure 2: Comparison of the flow pattern at time $t = 75s$. Relative differences of the density perturbation ϱ. Left immersed boundary - multidomain, right porous - multidomain.

variable	multidomain	porous	immersed boundary
ϱ	4.34×10^{-2}	4.02×10^{-2}	4.04×10^{-2}
difference	0%	7.3%	6.9%
u_1	2.13×10^{-3}	2.11×10^{-3}	2.11×10^{-3}
difference	0%	0.9%	.9%
u_2	3.23×10^{-4}	2.95×10^{-4}	2.97×10^{-4}
difference	0%	8.7%	8.0%

Table 1: Maxima of the computed quantities and relative differences to the multidomain case.

tions $x = 0$ (top of the hill) and $x = 52$ (end of the domain) are shown. The profiles for BC1 and BC2 are practically the same. The wavelength is given by the Brunt–Väisälä frequency and is the same for all BC. The boundary layer in the case BC1,2 is a little thinner with higher maximum on the top of the hill.

6. Conclusion

The flow around obstacle and over the hill in the stratified flow was simulated. Three different models of obstacle and three different outlet boundary conditions were implemented and compared.

Presented results show suitability of all models for modeling of this type of problems. Both wave structure far away the obstacle and boundary layer are well resolved. The flow pattern is practically identical for all obstacle models. The number, position and wave length are practically the same. While the u_1–velocity component is similar in all models (including the boundary layer), greatest differences are in the prediction of the u_2–velocity component. The more significant differences are mainly close to the corners and in the case of permeable model in the wake close to the obstacle. The boundary layer on the sides of the obstacle is resolved well in all cases.

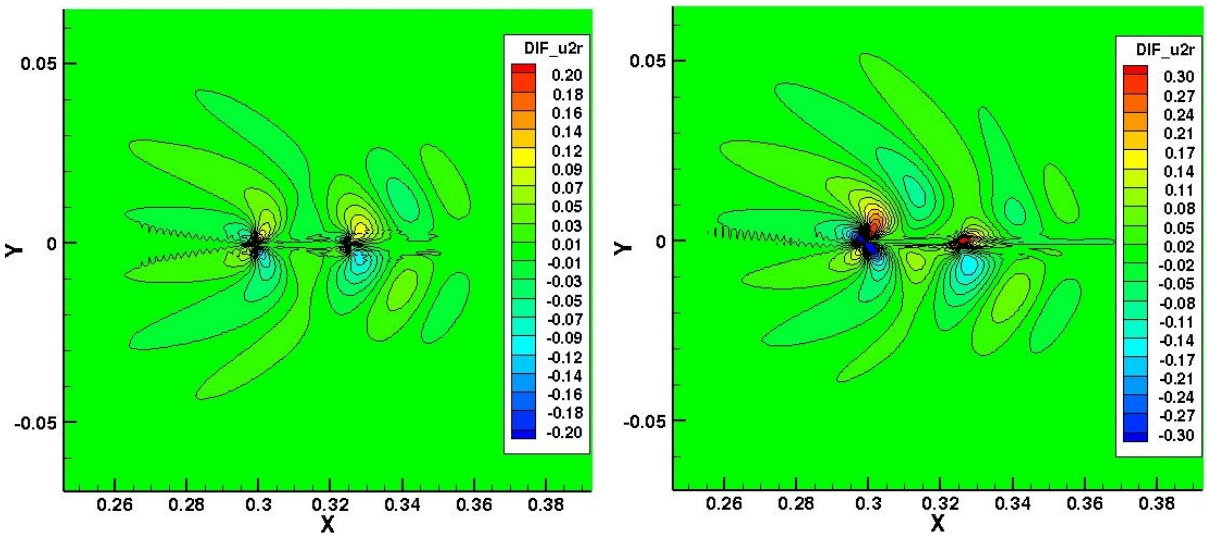

Figure 3: Comparison of the flow pattern at time $t = 75s$. Relative differences of the u_2 velocity component. Left immersed boundary - multidomain, right porous - multidomain.

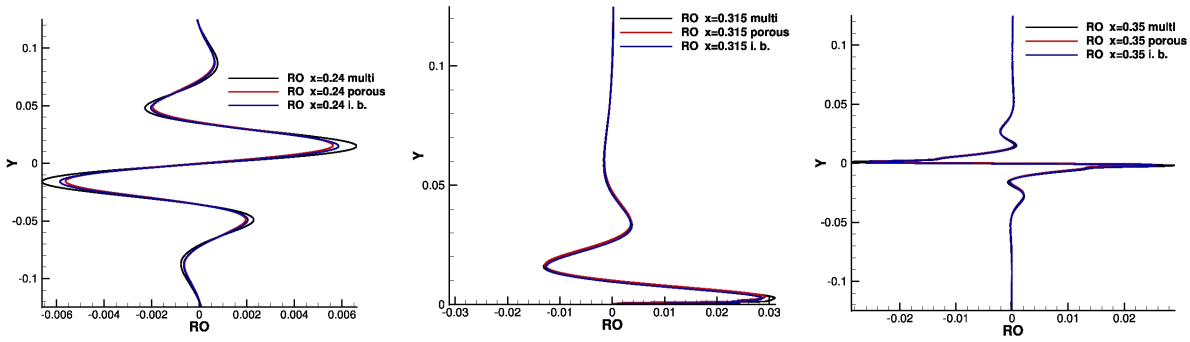

(a) $x = 0.24m$ (b) $x = 0.315m$ (c) $x = 0.35m$

Figure 4: Vertical profiles of the density perturbation ϱ in the different distances.

In the case of boundary conditions, the flow was significantly influenced by the boundary condition for pressure on the outlet.

For the deeper understanding of the behavior of these models and boundary conditions (e.g. dependency on the mesh density) further research is necessary.

Acknowledgments: This work was supported by TACR Project TA01020428 and grant CTU SGS13/174/OHK2/3T/12.

7. References

[1] Boyer D., Davies P., Fernando H., Zhang X.: Linearly stratified flow past a horizontal circular cylinder. *Phil. Trans. R. Soc. Lond.* **A328**, 501-528, 1989.

[2] Chashechkin Y., Gumennik E., Sysoeva E.: Transformation of a density field by a three-dimensional body moving in a continuously stratified fluid. *J. Appl. Mech. Tech. Phys.* **36(1)**, 19-29, 1995.

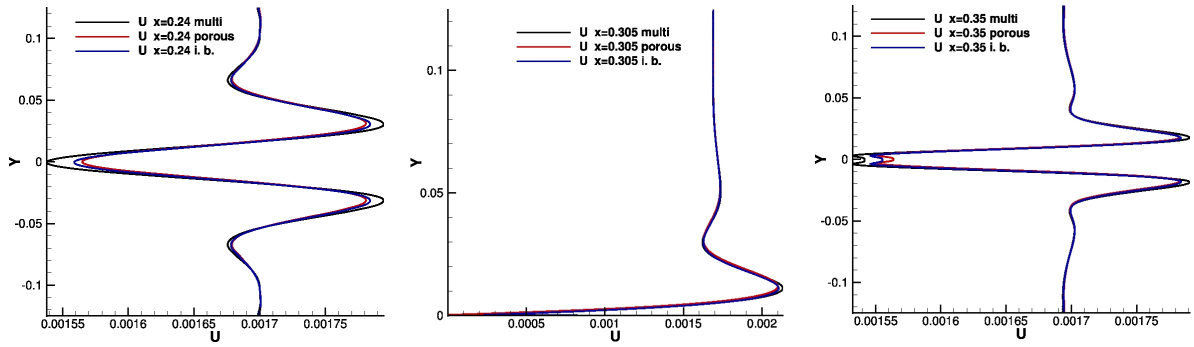

(a) $x = 0.24m$ (b) $x = 0.305m$ (c) $x = 0.35m$

Figure 5: Vertical profiles of the u_1–velocity component in the different distances.

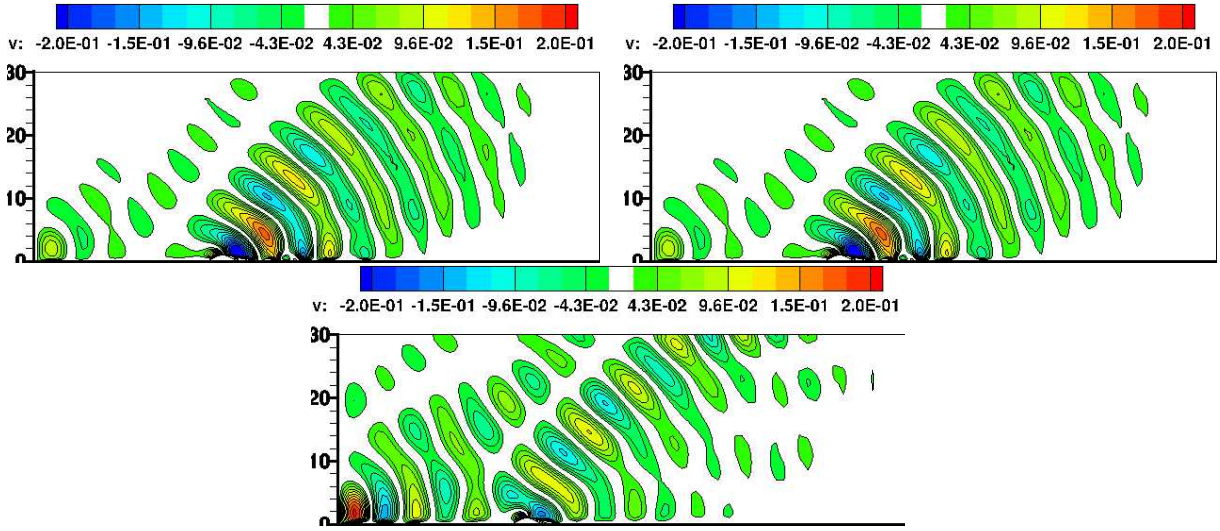

Figure 6: Gravity waves pattern for three different boundary conditions. BC 1 – top left, BC 2 – top right, BC 3 – bottom.

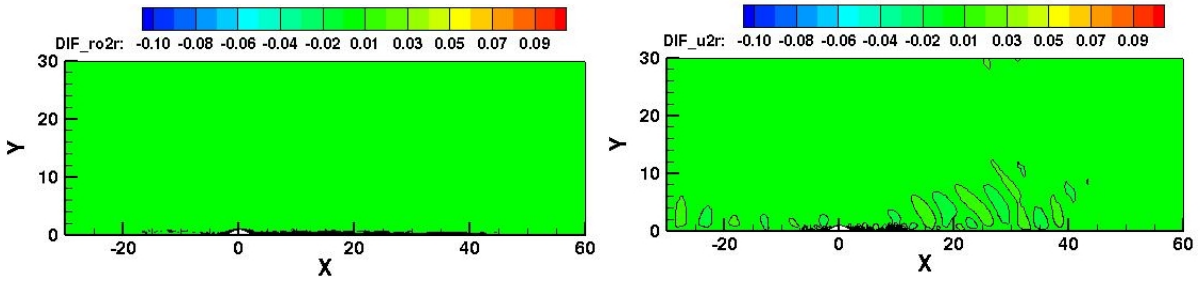

Figure 7: Relative differences of the density perturbance ϱ (left) and u_2–velocity component (right). Case BC3-BC2.

[3] Meunier P., Spedding G.: Stratified propelled wakes. *J. of Fluid Mech.* **552**, 229–256, 2006.

[4] Hanazaki H., Kashimoto K., Okamura T.: Jets generated by a sphere moving vertically in a stratified fluid. *J. of Fluid Mech.* **638**, 173–197, 2009

[5] Sutherland B., Linden P.: Internal wave excitation from stratified flow over a thin barrier. *J.*

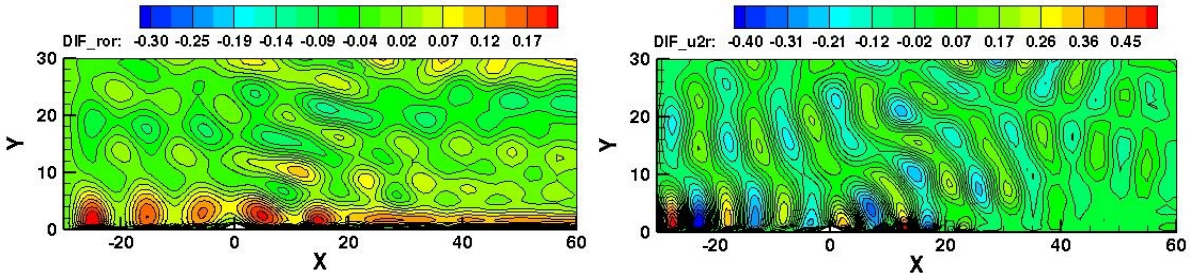

Figure 8: Relative differences of the density perturbance ϱ (left) and u_2–velocity component (right). Case BC3-BC1.

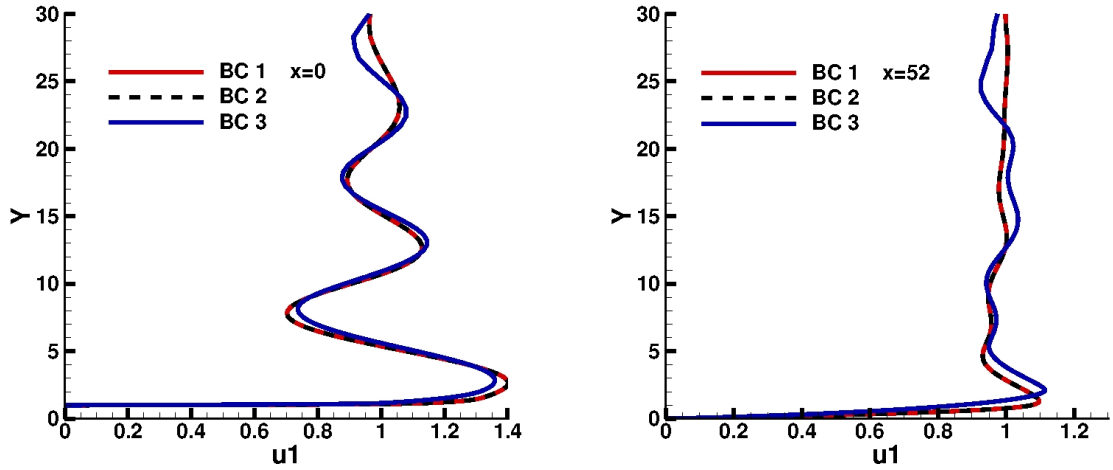

Figure 9: Profiles of u_1 velocity component in y-direction for $x = 0m$ (left) and $x = 52m$ (right).

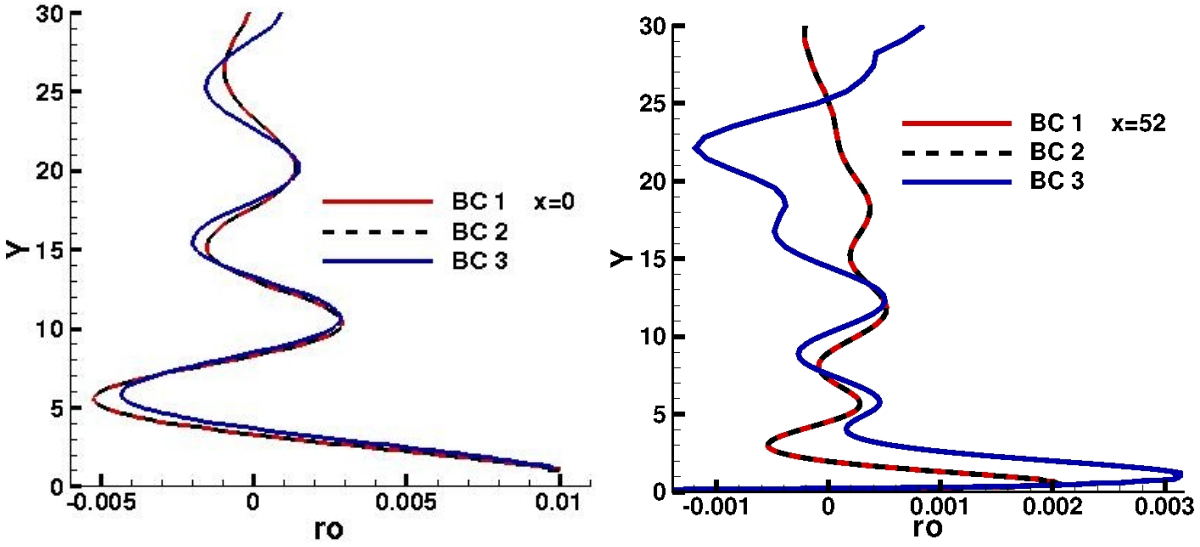

Figure 10: Profiles of density perturbation ϱ in y-direction for $x = 0m$ (left) and $x = 52m$ (right).

Fluid. Mech. **377**, 223-252, 1998.

[6] Brown S.: Slow Viscous Flow of a Stratified Fluid Past a Finite Flat Plate. *Proc. Royal Soc. Lond.* **306 (A)**, 239-256, 1968.

[7] Castro I.: Weakly stratified laminar flow past normal flat plates. *J. Fluid Mech.* **454**, 21-46, 2002.

[8] Bodnár T., Beneš L., Fraunié Ph., Kozel K.: Application of compact finite–difference schemes to simulations of stably stratified fluid flows. *A*pplied Mathematics and Computation, in press, DOI:10.1016/j.amc.2011.08.058 .

[9] T. Bodnár, L. Beneš, Ph. Fraunié, K. Kozel Application of compact finite-difference schemes to simulations of stably stratified fluid flows. Applied Mathematics and Computation **doi:10.1016/j.amc.2011.08.058** Article in press.

[10] Dick E., Vierendeels J., Riemslagh K.: A multigrid semi–implicit line–method for viscous incompressible and low–mach–number flows on high aspects ratio grids. Journal of Computational Physics **154** 310–341 (1999)

[11] Lele S.K.: Compact finite difference schemes with spectral–like resolutions. *J*ournal of Computational Physics 103(1992) 16–42.

[12] Beneš L., Fürst J., Fraunié Ph.: Numerical simulation of the towing tank problem using high order schemes. BAIL 2008 - Boundary and Interior Layers. Lecture Notes in Computational Science and Engineering 69, Springer 2009 ISSN 1439-7358.

[13] Beneš L., Fürst J.: Numerical simulation of the Stratified Flow Past a Body. *Numerical Mathematics and Advanced Applications. ENUMATH 2009.* Berlin: Springer, 2010, p. 155-162. ISBN 978-3-642-11794-7.

[14] Beneš L., Fürst J., Fraunié Ph.: Numerical simulation of the stratified flow using high order schemes. *E*ngineering Mechanics, 16(1):39–48, 2009. ISSN 1210-2717.

[15] Beneš L., Fürst J., Fraunié Ph.: Comparison of two numerical methods for the stratified flow. *J*. Computers & Fluids,in press, doi:10.1016/j.compfluid.2011.02.003.

[16] Chaschechkin Y.D., Mitkin V.V.: Experimental study of a fine structure of 2D wakes and mixing past an obstacle in a continuously stratified fluid. *Dyn. Atmos. Oceans* 34, 165–187, 2001

[17] Mittal R., Iaccarino G.: Immersed Boundary Methods. *Annu. Rev. Fluid Mech.***37**, 239–261.

[18] Fadlun A.A., Verzicco R., Orlandi P., Mohd–Yusof J.: Combined Immersed–Boundary Finite–Difference Methods for Three–Dimensional Complex Flow Simulations. *J. Comp. Phys.*, **161**(2000), 35–60.

[19] Berrabaa S., Fraunié Ph., Crochet M.: 2D Large Eddy Simulation of Highly Stratified Flow: The Stepwise Structure Effect. *Advances in Computation: Theory and Practise*, **7**, 179–186, 2001. Nova Sc. Publishers.

[20] Hemker P.W., Koren B.: Multigrid, defect correction and upwind schemes for the steady Navier-Stokes equations. Numerical methods for fluid dynamics III; *Clarendon Press/Oxford University Press*, 1988, p. 153-170.

[21] Janowitz GS.: The slow transverse motion of a flat plate through a non-diffusive stratified fluid. In:*J. Fluid Mech.* **47. 1**,p.171-181. 1971.

[22] E. Arquis and J.P. Caltagirone: Sur les conditions hydrodynamiques au voisinage d'une interface milieu fluide - milieu poreux: application a la convection naturelle. C.R. Acad. Sci. Paris II 299 (1984), pp. 1–4.

[23] Bodnár T., Beneš L.,Kozel K.: Numerical simulation of flow over barriers in complex terrain, *Il Nuovo Cimento*, **31 C,** N. 5-6, p.619-632, 2008.